UCRL-96666
PREPRINT

EXPERIMENTAL RESULTS FROM TMX-U

Donald L. Correll
and the
TMX-U Experimental Physics Group

This paper was prepared for submittal to the
Course/Workshop on Physics of Mirrors,
Reversed Field Pinches and Compact Tori,
Varenna, Italy
September 1-11, 1987

August 1, 1987

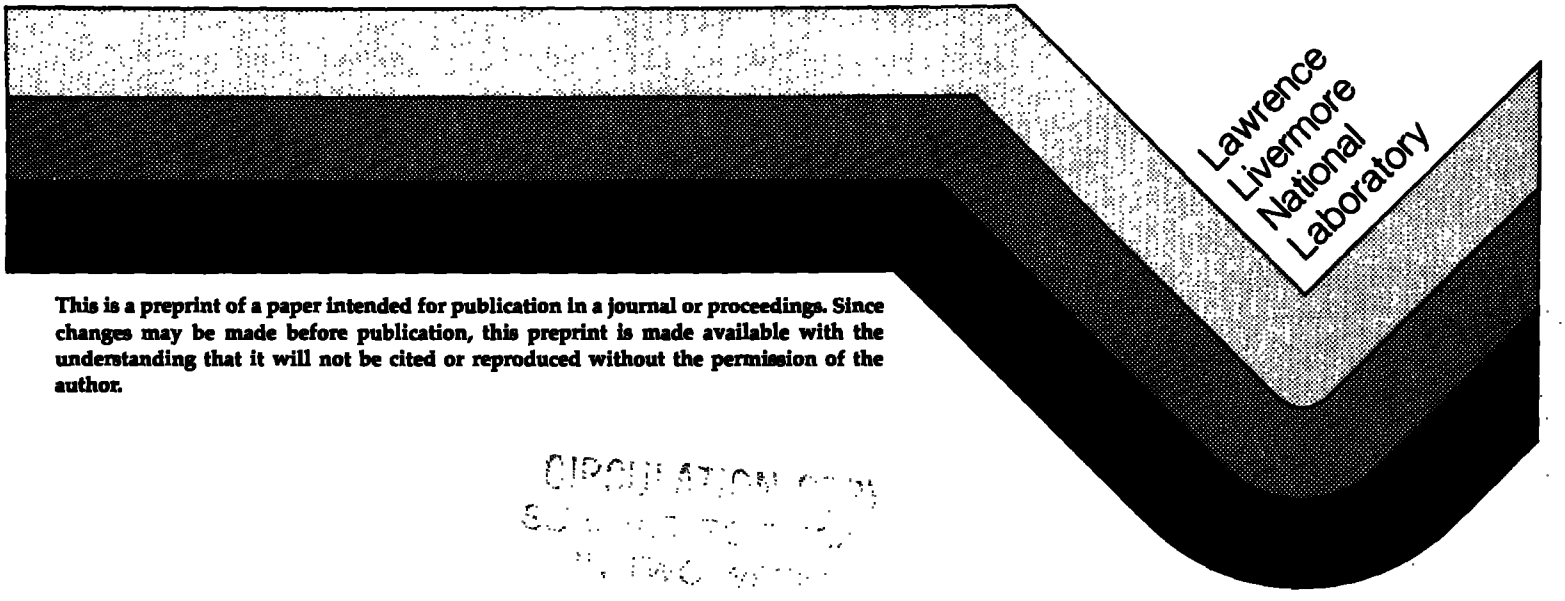

EXPERIMENTAL RESULTS FROM TMX-U*

Donald L. Correll and the TMX-U Experimental Physics Group

Lawrence Livermore National Laboratory, University of California
Livermore, CA 94550 U.S.A.

*This work was performed under the auspices of the U.S. Department of Energy by the Lawrence Livermore National Laboratory under contract number W-7405-ENG-48.

ABSTRACT

This paper presents the recent results [1] from the TMX-U experiment. Many of these results can be divided into two major areas: (1) axial confinement and plasma potential, and (2) radial transport and total confinement (i.e., particle balance). Among the key observations to be discussed are the following: When the ion-confining potential ϕ_{ic} is small, $\phi_{ic}/T_i \sim 1$-2, the axial confinement time scales as the theoretical Pastukhov time. Deep thermal barriers ($\phi_b \sim 0.7$ kV, $\phi_b/T_e \sim 6$-7) have been measured, but there is no strong correlation between ion-confining potential and the thermal-barrier depth. By installing a calibrated H_α emission diagnostic to measure the ionization current [2], we have quantified particle balance between the ionization source current and the four plasma current channels: (i) axial losses, (ii) nonambipolar radial losses, (iii) ambipolar radial losses, and (iv) density changes. All current channels are directly measured except for the ambipolar current, which is inferred from the particle balance equation. TMX-U operation above 1-3 x 10^{12} cm^{-3} is dominated by current channel (i) and below 1 x 10^{12} cm^{-3} by one or more of the remaining three channels. Central-cell particle buildup has been observed for one or two e-foldings and, within the radial core, found consistent with particle balance.

I. INTRODUCTION

The Tandem Mirror Experiment-Upgrade (TMX-U), which operated from early 1982 to late 1986 at the Lawrence Livermore National Laboratory (LLNL), was designed to investigate a complete thermal-barrier, tandem mirror system [3]. The TMX-U facility contains five major systems: (1) magnet; (2) vacuum; (3) heating, which includes neutral beams, electron cyclotron resonance heating (ECRH), and ion cyclotron resonance heating (ICRH); (4) neutral gas fueling; and (5) diagnostic. Figure 1 illustrates the TMX-U magnet-coil arrangement; the vacuum vessel; the location and orientation of the neutral-atom beams, ECRH, and ICRH; the gasbox; and the key particle balance diagnostics. The central cell has a magnetic field strength of 0.3 T, and each east and west end-cell magnet set generates a 2-T quadrupole-mirror field having a 4:1 mirror ratio. The design of TMX-U was based on a standard tandem mirror experiment, TMX [4], that was dismantled before building TMX-U. To improve the standard tandem mirror geometry, we designed TMX-U to test the use of "sloshing" ions to improve microstability and the production of an electron thermal barrier to optimize ion-confining potential formation.

Sloshing ions are magnetically trapped ions spending much more time at the axial boundaries of their movements within the end-cell magnetic field, which leads to a density maximum at their turning point. A thermal barrier is a depression in the potentially confined electron density at the end-cell midplane generated by magnetically trapped electrons, which leads to a potential minimum. The two hardware components required to establish sloshing ions and the thermal barrier in TMX-U are neutral beams aimed at skewed angles (47° and 40°) to the magnetic field axis and ECRH gyrotrons operating at 28 GHz. Gyrotrons exist at two locations in each end cell: the second harmonic location at the midplane (B = 5 kG) and the fundamental location near the outer turning point of the sloshing ions (B = 10 kG). The thermal-barrier, axial potential profile is determined by quasineutrality between both magnetically and potentially trapped species of ions and electrons within the end cells.

During 1982 and 1983, the production of sloshing ions [5] was verified, and the thermal-barrier potential profile [6] was initially measured. While investigating how to extend thermal-barrier operation from a central-cell (CC) density of 10^{12} cm^{-3} to 10^{13} cm^{-3}, the TMX-U group focused on two major issues: (1) axial confinement and plasma

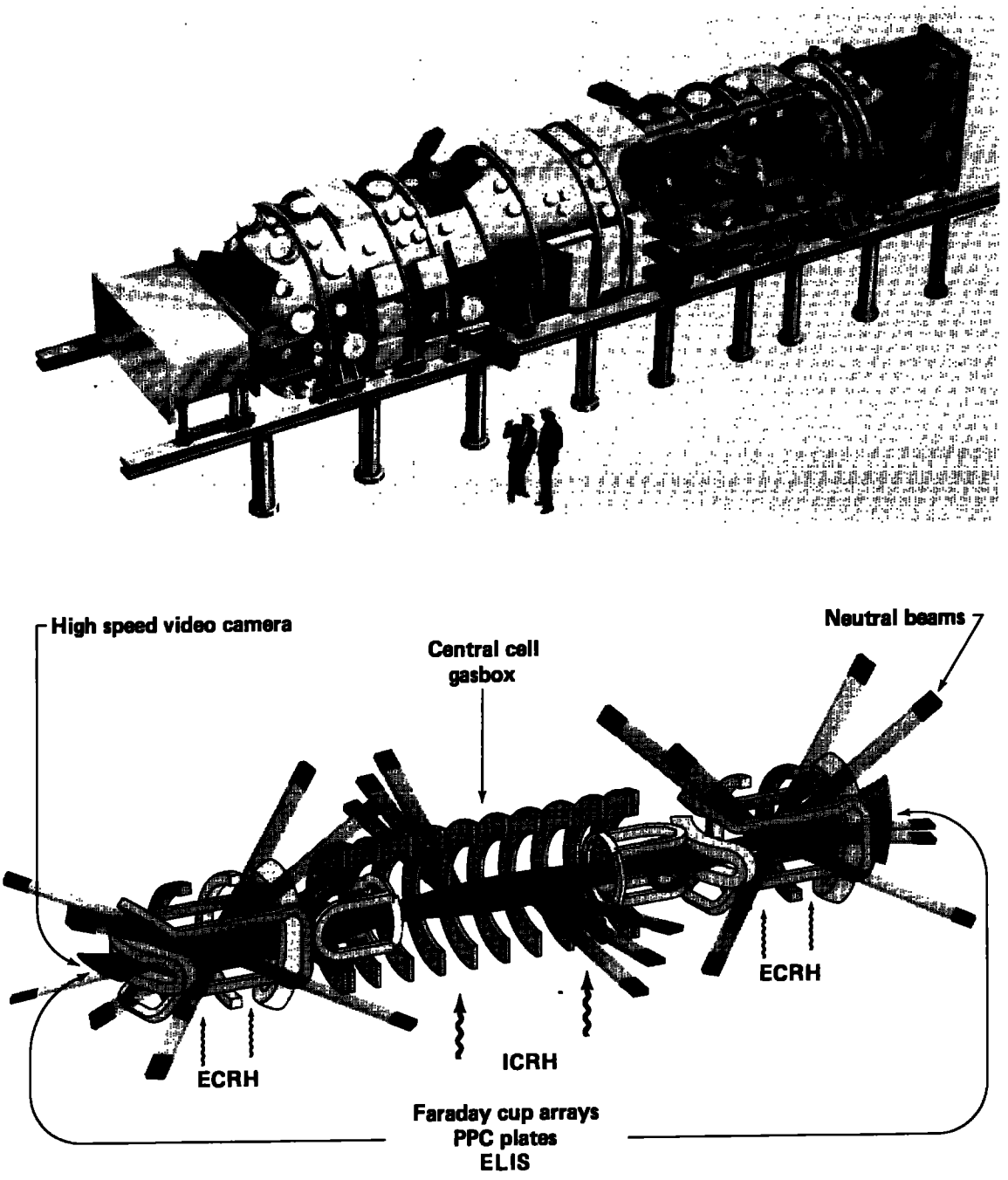

Figure 1. This figure shows the TMX-U vacuum vessel, the location and orientation of the heating and fueling systems, the arrangement of the magnets, and the key particle balance diagnostics.

potential measurements, and (2) radial transport and total confinement (i.e., particle balance). MHD and microstability studies within the CC and end-cell regions were carried out concurrently with both physics investigations.

In addition to these physics investigations, our major accomplishments with TMX-U were to:

- Develop neutral beam, ion cyclotron, and electron cyclotron plasma heating methods [1,7];
- Demonstrate improved ion microstability of a mirror plasma with sloshing ions [8];
- Increase maximum plasma temperature, potential, and confinement values in TMX-U relative to TMX;
- Demonstrate a thermal-barrier configuration at a density of a few 10^{12} cm^{-3}; and
- Develop diagnostics specific to studies of thermal-barrier plasmas.

TABLE I compares the maximum CC parameters achieved in TMX-U to those achieved in TMX [4,9]. The parameters of TABLE I were not achieved simultaneously on one given shot but are provided to illustrate the maximum operating regime of the two experiments. The maximum density n_c and the maximum density with enhanced axial confinement represent nonthermal-barrier and thermal-barrier operation, respectively, for TMX-U. The global energy confinement product includes the stored energy and radio-frequency (rf) powers of the two end cells as well as the central cell. TABLE I indicates that the major shortcoming in the TMX-U parameters was the CC density at which electrostatically enhanced axial confinement over magnetic alone could be demonstrated. Nevertheless, the electrostatic enhancement in axial confinement for TMX-U exceeded the TMX value by more than a factor of 5.

TMX-U demonstrated the ability to generate the thermal-barrier axial potential profile. The axial confinement of the central cell was enhanced (typically by 10 to 20 times the ionization fueling time, ≈ 5 ms) from the resulting electrostatic confining potential. For a small but finite number of shots and operating days, certain heating and fueling scenarios led to long axial confinement times (i.e., plugging) and concurrently to long radial confinement times (3 or more times the fueling time) so that particle buildup occurred with the CC density e-folding at a rate equal to the ionization rate. Particle buildup could only be sustained for one or

TABLE I. Comparison of maximum central-cell plasma parameters achieved in TMX and TMX-U[a]

	TMX	TMX-U
Maximum density, n_c (10^{13} cm^{-3})	3	1
Maximum density with enhanced axial confinement (10^{13} cm^{-3})	0.5	0.1-0.3
Maximum electron temperature, T_{ec} (keV)	0.1	0.28
Average ion temperature, T_{ic} (keV)		
Parallel	0.1	0.4
Perpendicular	2.5	2.5
Ion-confining potential, ϕ_{ic} (kV)	0.3	>1
Axial particle confinement product, $n\tau_p$ (10^{11} cm^{-3} s)	1	2
Electrostatic enhancement in axial confinement	9	50
Global energy confinement product, $n_e\tau_E^{global}$ (10^{10} cm^{-3} s)	1	2

From: G. D. Porter, Ed., TMX-U Final Report, Lawrence Livermore National Laboratory, Livermore, CA, UCID-20981 (1987).

[a]These parameters were not achieved simultaneously on one shot.

two e-foldings up to a CC density of 10^{12} cm^{-3}, at which time the axial confinement degraded (i.e., plugging was lost). Loss of plugging refers to the degradation of axial confinement from over ten times the ionization fueling time to approximately equal to the ionization fueling time.

During thermal-barrier operation, mirror-confined and potentially confined ions and electrons were produced and, within the operating density limits, satisfied the thermal-barrier requirements. However, the velocity distributions and/or lifetimes associated with the end-cell species could not be fully controlled by the existing neutral beam and ECRH hardware. Detailed results of the physics associated with sloshing ions and hot electrons within the TMX-U end cells are presented in Refs. [8] and [10]. In the next section (Sec. II), we discuss the thermal-barrier axial potential profile, supporting potential diagnostics, and the resulting axial confinement. Section III discusses radial transport, key particle balance diagnostics, and the resulting total confinement.

II. AXIAL CONFINEMENT AND POTENTIAL PROFILE MEASUREMENTS

This section describes the axial structure of the thermal-barrier potential profile and its role in determining axial confinement.

A. Expected Thermal-Barrier Potential Profile

Linear (e.g., mirror) confinement geometries, unlike toroidal (e.g., tokamak) confinement geometries, can support large density gradients along the magnetic field lines. Potential changes along field lines in mirror machines can be on the order of or larger than the electron temperature. When mirror-confined electrons are absent, the relationship between density and potential is given by the Boltzmann relationship

$$e\phi(z) = T_e \ell n \frac{n(z)}{n} \quad . \tag{1}$$

When mirror-confined electrons, n_e^{hot}, are present, only the potentially confined fraction of the total electron density, n_e, contributes to the potential, ϕ. Figure 2 defines the expected density and potential axial profiles for the thermal-barrier geometry, where n_{si} is the sloshing-ion density; n_c is the CC density; f_e^{hot} is n_e^{hot}/n_e, z = b is the axial position of the thermal-barrier potential minimum (nominally the midplane of the end cell with B = 5 kG for TMX-U); and z = a is the axial position of the potential maximum (nominally the outer turning point of the sloshing ions having a TMX-U design value of B = 10 kG). The CC potential, ϕ_{ec}, with respect to the end wall is set by the requirement that loss currents of ions and electrons must be equal. The barrier depth, ϕ_b, and the peak potential height, ϕ_p with $\phi_a = \phi_p - \phi_b$, are set by the requirement of quasineutrality between the total sum of magnetically and potentially trapped ions and electrons [11]. The CC ion-confining potential, ϕ_{ic}, is given by

$$\phi_{ic} = \phi_a - \phi_b \quad . \tag{2}$$

Assuming the electron density at z = a is set by the sloshing ions and defining $(1 - f_e^{hot})$ as the fraction of potentially confined electrons at z = b, we can functionally describe ϕ_{ic} by [1]

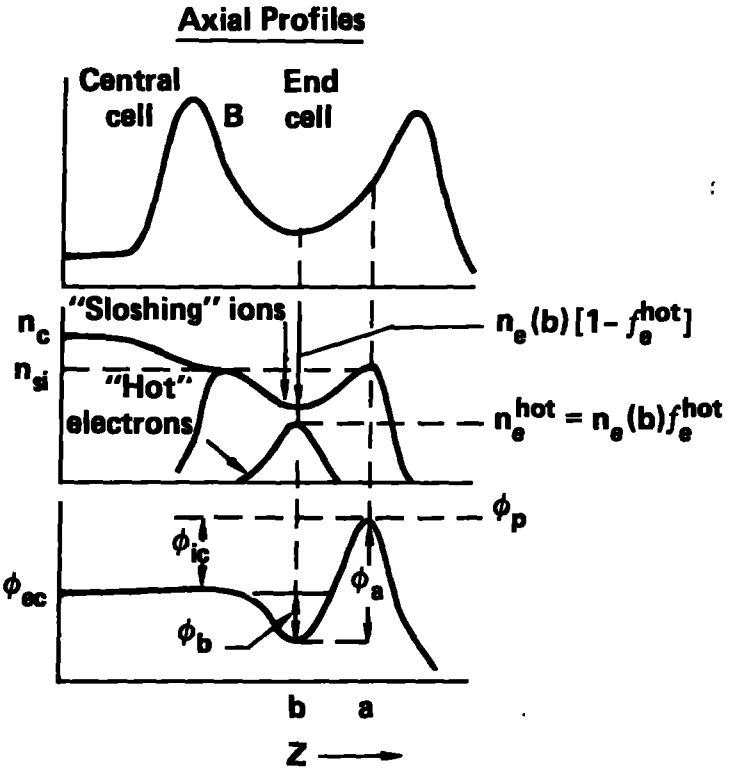

Figure 2. The expected density and potential axial profiles for the thermal-barrier geometry.

$$\phi_{ic} \propto T_{ec} \left[\frac{n_{si}(a)}{n_e(b)\ (1 - f_e^{hot})} \right]^{2/3} - \phi_b \ . \qquad (3)$$

Equation (3) establishes the importance of the sloshing ions [8] and the fraction of mirror-confined electrons [10] to the thermal-barrier geometry.

B. Measured Thermal-Barrier Potential Profile (Diagnostics and Results)

Figure 3 shows the axial profile of the magnetic field, the expected axial profile of the potential, and the measurement location of the plasma potential diagnostics. The CC plasma potential diagnostic (PPD) is a heavy-ion beam probe that determines the potential at the midplane of the central cell [1,7]. The time-of-flight (TOF) analyzer is a charge-exchange analyzer that measures the velocity distribution function of

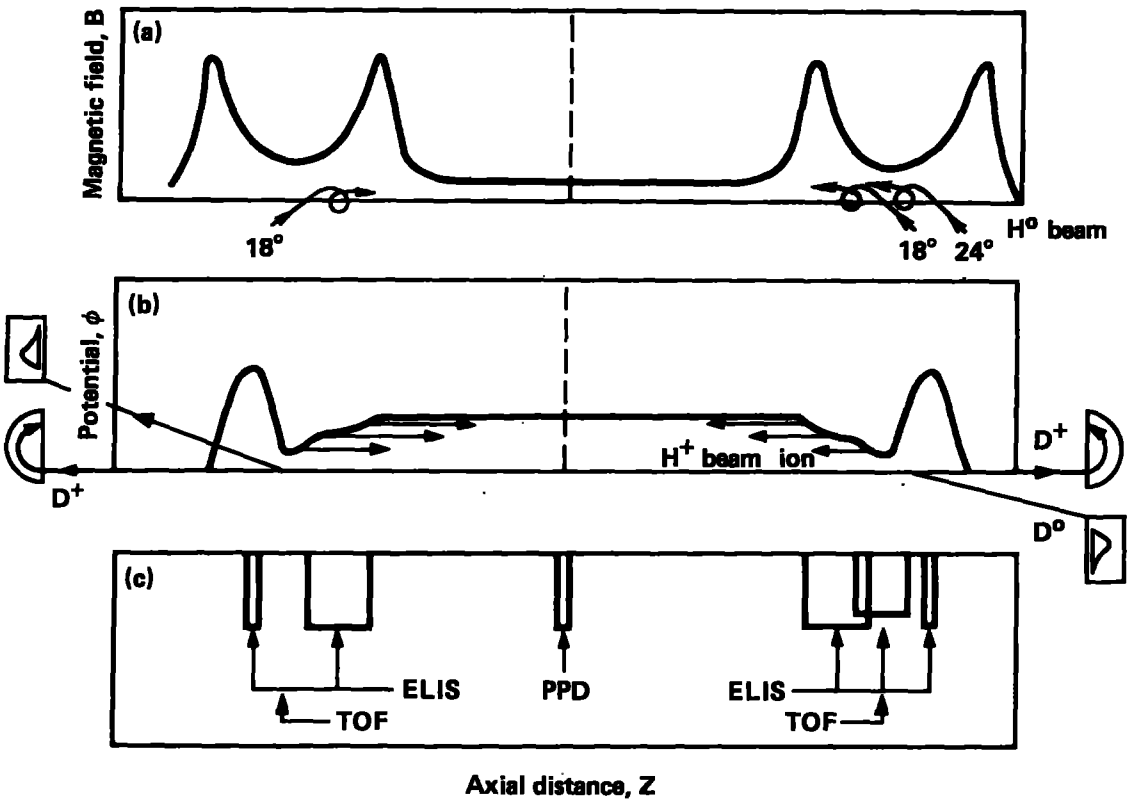

Figure 3. The axial measurement location (c) of the TMX-U potential diagnostics referenced with respect to the TMX-U magnetic field (a) and expected axial potential profile (b).

neutral particles (D°) emitted from the thermal barrier with kinetic energy in the range 50 eV < E < 1500 eV and with a pitch angle of 22.5°. Examination of this distribution function permits identification of phase space boundaries, which in turn determine the potential difference, ϕ_b, between the end-cell inner mirror and the barrier, and the potential difference, ϕ_a, between the barrier and the peak potential, ϕ_p [12]. The end-loss ion spectrometer (ELIS) measures the energy spectrum of the ions, D^+, that are lost axially [13]. Besides examining the ions leaving the end-loss plasma out the ends of TMX-U to determine ϕ_p, we sampled the plasma potential in certain regions of the end cells with three diagnostic neutral-beam probes (formerly used as pump beams [1]). The squiggles and broad rectangles in Fig. 3 show the measurement location of the two 18° (one per end cell) and the one 24° (west end cell only) diagnostic (pump) beams. All three diagnostic beams were normally operated on H_2 (H° injection) to help differentiate the H^+ beam ions from the D^+ plasma ions.

Because the injection angles are shallow with respect to the magnetic axis and therefore lie within the mirror loss cone, any of the energetic diagnostic-beam atoms ionized by the plasma in an end cell can travel through TMX-U and out the other end. These ions arrive at the electrically grounded ELIS with energy equal to their original beam energy, E_b, plus the energy, $e\phi$, corresponding to the plasma potential in the region where they were born. Thus, knowing the original beam energy determines the plasma potential.

If plasma potential data from the ELIS are plotted against the axial location of the diagnostic neutral beams within the west end cell, then a strong case for a thermal-barrier potential depression can be made (Fig. 4). Three potentials are determined from diagnostic beam 6F (18°) injected near the inner sloshing-ion turning point (z ≈ 5 m). The first, which is the one usually obtained, is determined by finding the energy of the centroid of the signal from the half and one-third energy components

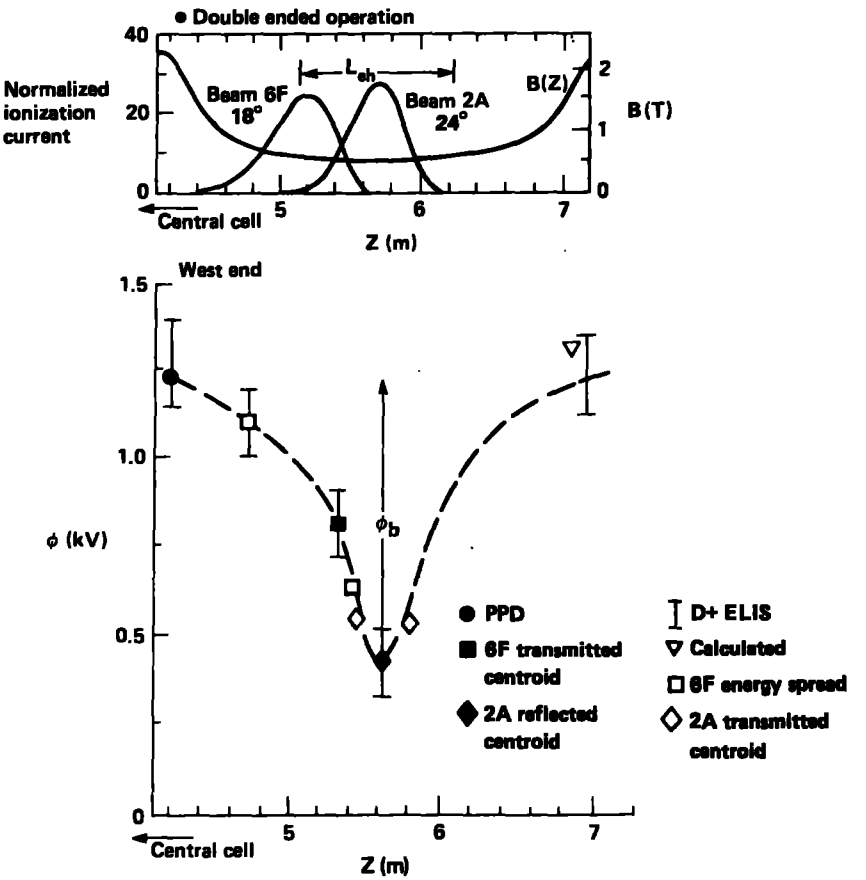

Figure 4. The end-cell, axial potential profile measurements at 44 ms on shot 16, August 13, 1986.

of the beam. We assume that this energy determines the potential at the peak product of plasma density and beam density. Hence, it determines the potential at z = 5.2 m, i.e., ϕ (5.2) = 0.8 kV. The other two points from beam 6F, an estimate of the potential extrema over the beam footprint, are determined using the energy spread in the signal. Two additional points on the axial profile were obtained from diagnostic beam 2A (24°) aimed at the barrier midplane (z ≈ 5.6 m). The minimum potential is found by measuring a signal on the west ELIS from a reflected portion of beam 2A. This signal arises because of the large thermal-barrier depth. The condition for the existence of a reflected signal from the one-third energy component ($E_b/3$), which arises from the break-up of extracted molecules, depends on the barrier depth and the barrier mirror ratio [1]. The potential obtained from this measurement is indicated by the solid diamond in Fig. 4 and is assumed to be at the barrier midplane. The second potential obtained from this beam is determined from the energy shift of the centroid of the transmitted beam and is shown as the open triangles in Fig. 4. This potential is about 0.1 kV higher than that measured on the reflected signal. Although no direct method of determining the axial location of the transmitted beam source exists, we assume the potential minimum is located at the magnetic field minimum. Because the transmitted beam indicates a higher potential than the reflected beam, the data are plotted slightly off the midplane.

The existence of the deep thermal barrier depends strongly on the second harmonic ECRH power at z = b, B = 5 kG. Available data similar to Fig. 4 indicate that the barrier depth, between 0.5 and 0.75 kV, rapidly vanishes when the second harmonic ECRH power is turned off. The barrier depth decreases much more rapidly than the decay rate of the hot electrons detected by the diamagnetic loops and x-ray detectors in the end cell. The hot electrons typically decay under most circumstances with a time constant from ~10 to 100 ms. However, the thermal-barrier potential drops dramatically in the time between samples on the ELIS, every 0.2 ms. This difference in decay times suggests that the thermal-barrier potential is being determined by a low-energy, magnetically confined electron species [1,10].

Also in Fig. 4, note that the thermal-barrier depth, ϕ_b = 0.8 kV, which is one of the deepest values observed on TMX-U, was measured during a shot with marginal axial confinement, $\tau_{\parallel}$. The ion-confining potential ($\phi_{ic} = \phi_a - \phi_b$), as discussed in Fig. 2, which would be consistent with

electrostatic confinement, $\tau_{\parallel} \propto \exp \phi_{ic}/T_{ic}$, would indicate $\phi_{ic}/T_{ic} \approx 1$. The calculated value, indicated by a triangle in Fig. 4, is consistent with the potential inferred from the low-energy D^+ spectrum on the west ELIS.

The existence of the very deep thermal barrier, $\phi_b/T_{ec} \approx 6\text{-}7$, on a shot with marginal axial confinement indicates that the axial confinement is not necessarily determined uniquely by the physics of the thermal-barrier depth, ϕ_b. This observation should not be too surprising since $\phi_a - \phi_b = \phi_{ic}$ determines axial confinement. Nevertheless, there should be good thermal isolation between the CC electrons and the warm, potentially confined electrons within the ϕ_a electron well. Thus, the fundamental ECRH at z = a, B = 10 kG, together with the sloshing ions, should provide an ion-confining potential. Because of these data and results from other shots where $\tau_{\parallel}$ does not scale with ϕ_b [1], we believe that some of the difficulty in obtaining good axial confinement in TMX-U lies with the absorption of the fundamental ECRH power and the axial profile of the sloshing ions.

Next, we discuss axial confinement and potential profiles, with emphasis on TOF measurements of ϕ_a and ϕ_b, which are used to compare measured and expected $\tau_{\parallel}$.

C. Axial Confinement and Potential Profiles

Axial confinement refers to the axial particle lifetime of the CC ions,

$$\tau_{\parallel} = q \frac{N}{I_{\parallel}} \quad , \tag{4}$$

where the total number of CC particles, N, is given by the CC parameter product $\hat{n}_c \pi r_c^2 L_c$; the axial end-loss current of ions, $I_{\parallel}$, is determined from the Faraday cup (FC) arrays at both ends of the machine; and q is the electron charge. For diagnostic reasons, $\tau_{\parallel}$ is evaluated for the CC plasma core ($r_c \lesssim 10$ cm). Uncertainties and changes in the radial profiles for n(r) and I(r) have a relatively smaller effect on $\tau_{\parallel}$ for the core compared to the value associated with the plasma column out to the CC limiter. A Gaussian e-folding radius, $r_0 = 20$ cm, and a parabolic cutoff radius equal to the CC limiter radius, a = 25 cm, give similar results for $\hat{n}$ from microwave interferometer measurements.

An electrostatically enhanced value of $\tau_{\parallel}$ is synonymous with the term "plugging." Several definitions of plugging exist, but the following seem to be widely accepted:

1. Strong plugging is defined as $\tau_{\parallel} > 20$ ms. The ELIS diagnostic has signal-to-noise problems determining potentials when the axial end losses are lower than the value of $I_{\parallel}$ associated with $\tau_{\parallel} \gtrsim 40$ ms.
2. Moderate plugging is defined as $10 < \tau_{\parallel} < 20$ ms. A $\tau_{particle} \geq 10$ ms was predicted by particle buildup calculations as the critical value required for neutral-beam buildup within the central cell [1].
3. Partial plugging is defined as $5 < \tau_{\parallel} < 10$ ms. For TMX-U CC length, $L_c = 510$ cm, and mirror ratio, $R_c = 22/3$, the theoretical predictions for unplugged axial confinement for $\phi_{ic} = 0$ (i.e., magnetic confinement only with no electrostatic enhancement) are 1 to 4 ms for densities, n_c, ranging from 5×10^{11} to 2×10^{12} cm^{-3} and ion temperatures, T_{ic}, ranging from 50 to 200 eV [1,7].

A very large fraction of the plugging and loss of plugging (LOP) studies on TMX-U were done with plasmas having n_c and T_{ic} as defined above. Therefore, strong plugging measurements of $\tau_{\parallel}$ from 50 to 100 ms are many times (greater than 10) the unplugged, $\phi_{ic} = 0$ values of 1 to 4 ms. LOP refers to the transition of $\tau_{\parallel}$ from plugging to unplugging values.

The relationship between axial confinement and potential profiles is explored by comparing the experimentally determined value of $\tau_{\parallel}$, Eq. (4), to the theoretically predicted value, $\tau_{\parallel}^{theory}$. For the TMX-U data discussed in this paper, the complete theoretical expression [14] can be approximated by the Pastukhov, collisionless limit

$$\tau_{\parallel}^{theory} \approx 2\, \tau_{ii} \left(\frac{\phi_{ic}}{T_{ic}}\right) \exp\left(\frac{\phi_{ic}}{T_{ic}}\right) , \qquad (5)$$

where $\tau_{ii} \approx 10^6\, T_{ic}^{3/2}$ (eV) is the 90° coulomb collision time for CC ions with temperature, T_{ic}; $\phi_{ic} = \phi_a - \phi_b$; and the factor of 2 is determined by the CC mirror ratio, $R_c = 22/3$, and by the range in ϕ_{ic}/T_{ic} values of $\gtrsim 1$ or 2. The familiar mirror ratio dependence for mirror confinement, τ_{ii} log R, is modified according to Eq. (5) because only ions with energy exceeding ϕ_{ic} can escape axially.

The TOF analyzer (Fig. 3) [12] can determine the input parameters to Eq. (5), $\phi_{ic} = \phi_a - \phi_b$ and T_{ic}. As discussed earlier, this instrument measures the velocity distribution of the flux of neutral atoms resulting from charge-exchange between ions within the thermal-barrier region of the end cell and neutral particles injected by the sloshing-ion beam. Figure 5 illustrates the various ion species for a thermal-barrier-type potential profile and gives a sample energy spectrum measurement from the TOF analyzer, which helps show how the TOF analyzer can be used to measure both ϕ_{ic} and T_{ic}. The TOF analyzer is collimated to accept charge-exchange neutrals from ions with a pitch angle of 22.5° with respect to the magnetic axis. Because this angle is less than the magnetic loss-cone angle associated with the mirror ratio, R = 4 of the

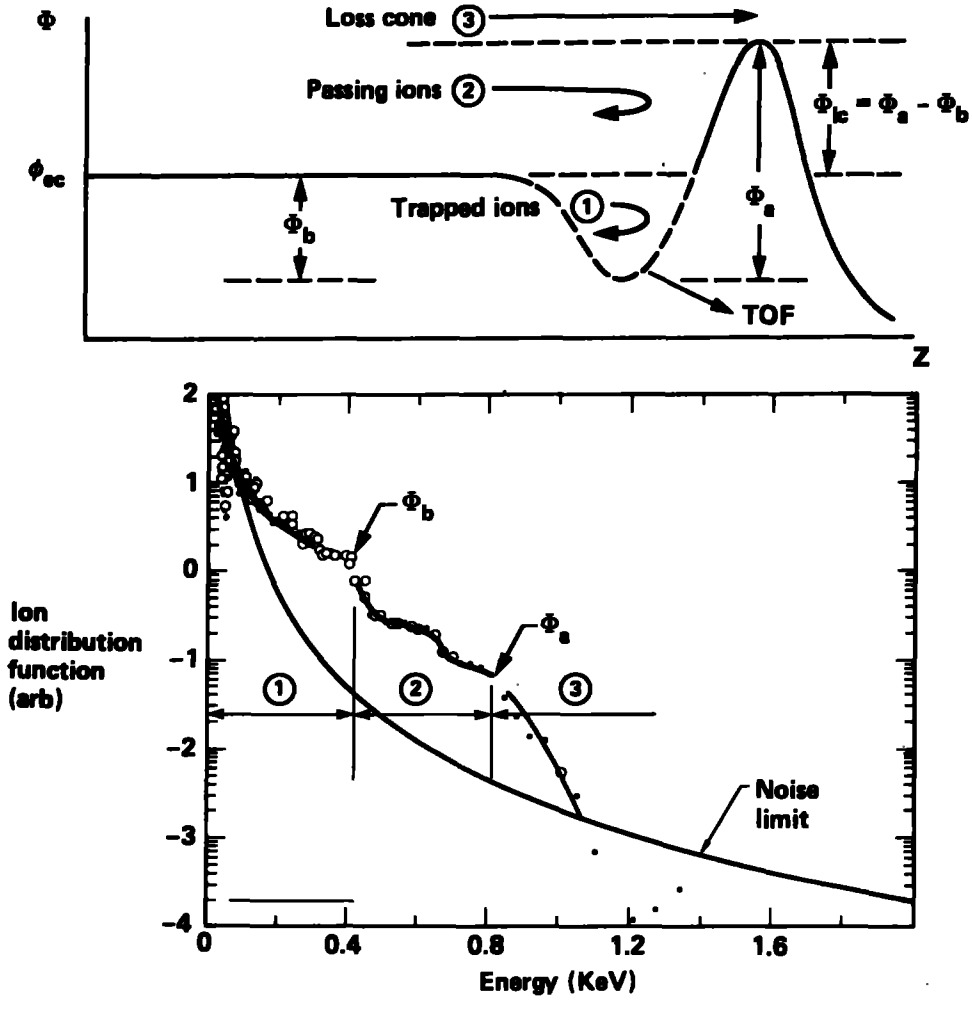

Figure 5. The interpretation of potential measurements with the time-of-flight (TOF) diagnostic.

end cell, $\sin^{-1}(1/\sqrt{R}) = 30°$, the velocity distributions of all three end-cell ions are measurable: (1) the trapped ions within the thermal-barrier potential; (2) the passing ions, which are confined by ϕ_{ic} and can pass between the central cell and the outer confining potential peak; and (3) the loss-cone ions from the central cell, which are not confined by the CC phase space boundary determined by ϕ_{ic} and R_c.

Each region of Fig. 5 with a different slope and associated break between adjacent regions corresponds to the ion velocity distribution of one of the three end-cell ion components. To convert a break, E_{br}, in the TOF spectrum of the ion velocity distribution to a potential difference, ϕ_a or ϕ_b, we must use Eq. (6):

$$\delta\phi = E_{br}\left(1 - \frac{B_\delta}{B_b}\sin^2 22.5°\right), \tag{6}$$

where $\delta\phi$ is either ϕ_a or ϕ_b, B_δ is the magnetic field at which the potential difference, ϕ_a or ϕ_b, reaches a maximum; B_b is the magnetic field at the thermal-barrier location (5 kG), and 22.5° is the TOF line-of-sight angle. By fitting the distribution within the passing ion region by a Maxwellian, the value of T_{ic} is determined.

Unfortunately, the interpretation of the TOF spectrum is sometimes not as straightforward as indicated in Fig. 5. The exact location of the outside potential peak on the outboard side of the end-cell midplane is not known. Frequently, there is evidence of a local inside potential maximum between the end-cell midplane and the magnetic field maximum on the inboard side of the end cell. Since the exact location of this inside potential maximum is also not well known, neither ϕ_a nor ϕ_b can be determined precisely. Nevertheless, a set of data from LOP studies on TMX-U allowed $\phi_{ic} = \phi_a - \phi_b$ and T_{ic} to be inferred from the TOF spectrum. That data set is plotted in Fig. 6.

Figure 6 compares the axial confinement time from the measurement of the CC plasma density and the ion end-loss current out the east end according to Eq. (4) to the calculated axial confinement time according to Eq. (5) based on the potential profile and CC ion temperature inferred from the TOF spectrum. These data are accumulated over several different shots. All data were taken during unplugged operations on the west end. For reasons not presently known, this single-sided plugging condition produced breaks within the TOF spectrum that were more easily

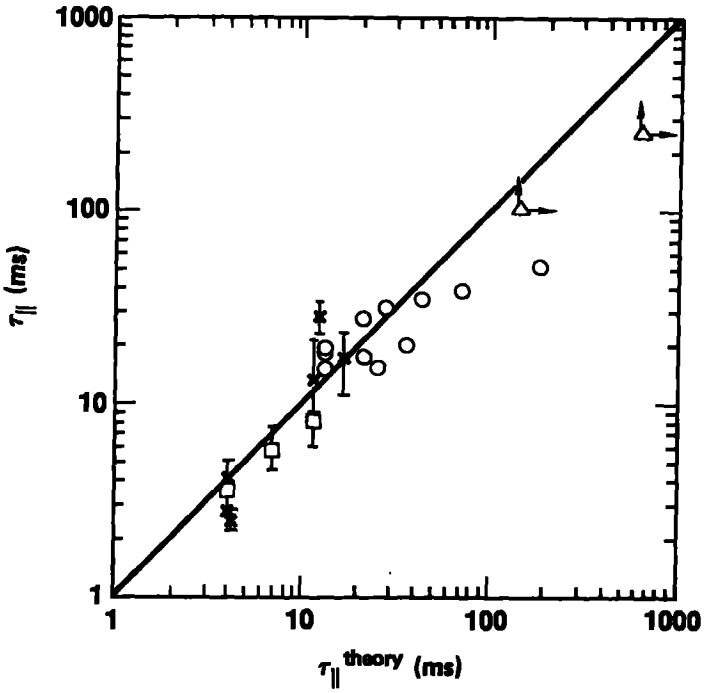

Figure 6. The experimentally measured axial confinement time, $\tau_{\parallel}$ [Eq. (4)] vs the theoretically predicted value, $\tau_{\parallel}^{theory}$ [Eq. (5)] using TOF-inferred values of ϕ_{1c} and T_{1c}.

identifiable. There are two important features of the TOF spectra in calculating the ion-confining potential. The low-energy break associated with ϕ_b in the spectrum of Fig. 6 is assumed to signify the start of the passing ions, to equal the potential difference between the thermal barrier and the inner mirror, and to occur at the inner mirror (B = 22 kG). The high-energy break associated with ϕ_a in the spectrum of Fig. 5 is assumed to represent the loss-cone boundary for the passing ions, to equal the potential difference between the thermal barrier and the ion-confining potential, and to occur at the outer end-cell mirror (B = 20 kG). The TOF-measured values of ϕ_{1c}/T_{1c} ranged from slightly less than 1 to almost 4. The CC ion temperature, T_{1c}, as inferred from the passing ion distribution was nominally 100 eV. The data show that under these circumstances the measured axial confinement time in TMX-U follows the expected Pastukhov axial confinement scaling given in Eq. (5).

III. RADIAL TRANSPORT AND TOTAL CONFINEMENT

Total ion particle confinement in TMX-U, as with other tandem mirrors, encompasses both axial transport and radial transport. As for the axial end losses, we also assume that the radial losses originate in the central cell. Radial losses in the end cell [15] associated with the ECRH and sloshing-beam heating systems can be present, but this additional complication need not be considered for the conclusions drawn in this paper. The following discussion follows closely a more complete presentation in Ref. [2].

A. Radial Transport and the Particle Balance Equation

Radial transport in a linear machine can manifest itself in two independent components: nonambipolar and ambipolar. A nonambipolar radial current (nonequal ion and electron radial fluxes) consists of radial ion losses being neutralized by axial electron losses to the end wall [16,17]. An ambipolar radial current (equal ion and electron radial fluxes) is not detectable directly with any charge-sensitive diagnostic; hence, the magnitude of current must be inferred from particle balance using the ion continuity equation [2]:

$$I_s = q\frac{dN}{dt} + I_{\parallel} + I_{\perp}^{NA} + I_{\perp}^{A} \quad , \tag{7}$$

where I_s is the ionization plasma-source current, similar to Eq. (4), N is the total number of CC particles with q the electron charge, $I_{\parallel}$ is the axial ion-loss current, $I_{\perp}^{NA}$ is the radial nonambipolar-loss current, and $I_{\perp}^{A}$ is the residual loss current required to balance the equation. A positive $I_{\perp}^{A}$ is attributed to outward ambipolar losses or measurement errors (e.g., errors due to incomplete radial or azimuthal profile measurements of particle losses). Although Eq. (7) is valid for a column of any radius, this discussion focuses on the plasma core (CC radius $r_c \lesssim$ 10 cm) because the uncertainty in I_s from the influence of molecular deuterium on the ionization source is the smallest in this region and because of the remarks following Eq. (4). A Z_{eff} coefficient is not needed in Eq. (7) because low impurity concentrations have been measured

($Z_{eff} \approx 1$) [2]. Figure 7 identifies schematically the terms of Eq. (7) as they apply to the TMX-U geometry.

B. Particle Balance Diagnostics

Figure 1 gives the location of the key particle balance diagnostics which we discuss next.

The measurements of the axial ion-loss current density are obtained at each end of TMX-U from a linear FC array equipped with biased grids (-3 kV) to repel electrons. The term $I_{\parallel}$ for the core is obtained by assuming azimuthal symmetry and integrating the FC data for the core flux tube as a function of time. The ELIS at each end measures the loss current vs energy and mass near the plasma axis ($r < 2$ cm) [13].

The net axial electron current is measured by radially and azimuthally segmented plasma-potential control (PPC) plates on each end wall [17]. These plates can be isolated from ground (10 kΩ to 1 MΩ) or grounded. The $I_{\perp}^{NA}$ term in Eq. (7) is inferred from the sum of the negative-electron current from the PPC plates that correspond to the core flux tube (see Fig. 7).

The time rate of change of the total number of particles dN/dt is calculated from line-density measurements by microwave interferometers and has the largest uncertainty of all the terms in Eq. (7). Several interferometers located in the central cell are used to obtain approximate axial and radial density profiles. As with the previous discussion of $\tau_{\parallel}$,

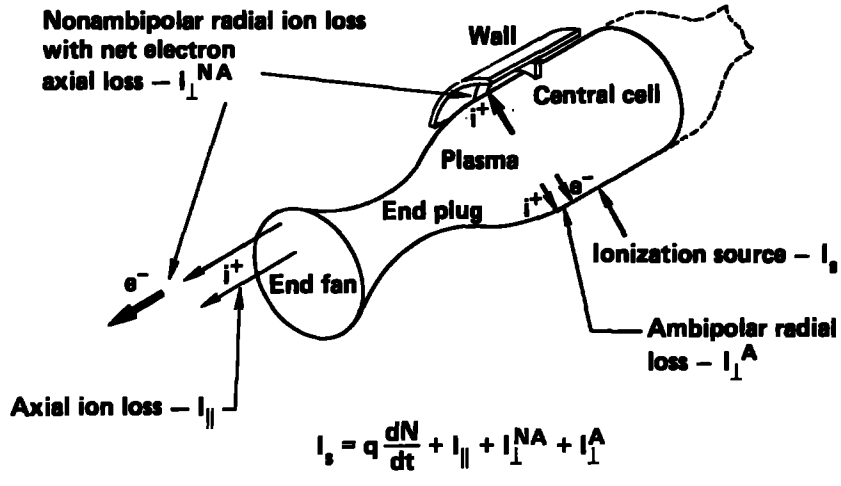

Figure 7. Particle sources and losses in a tandem mirror plasma.

the radial profiles in the central cell are approximated by a Gaussian with a 20-cm e-folding radius. The axial profile is assumed constant with an effective cylindrical flux-tube length, L_c = 510 cm in the central cell. The dN/dt term is calculated by $Vd(\hat{n})/dt$, where V is the core plasma volume (constant in time) and $\hat{n}$ is the on-axis density derived from the measured line density as indicated in the discussion following Eq. (4).

The ionization source I_s is obtained from absolutely calibrated measurements of atomic deuterium Balmer-alpha H_α emissions at 6561 Å. A high-speed (0.5 ms/frame), filtered (30-Å) video camera views the plasma column from the end of TMX-U. The linear geometry of the tandem mirror allows axial integration of the optically thin plasma emissions to obtain a two-dimensional (radial and azimuthal) measurement of the total source. Other camera systems located along the plasma column (viewing radially) showed that most of the ionization occurs close to the gas-box source located near the CC midplane where the plasma cross section is nearly circular. Reference [2] discusses how the optical system is absolutely calibrated and how the ionization current density is obtained by multiplying the measured H_α brightness by an atomic physics factor, R: the branching ratio between electron-impact ionization and electron-impact excitation followed by H_α emission. This R factor involves the ratio between two cross sections and, for the TMX-U core plasma, is relatively insensitive to electron temperature and density. The typical core plasma conditions of TMX-U (CC density in the 10^{12} cm^{-3} regime and an electron temperature of ~100 eV) indicate a value of R = 11 ionizations/photon [2] with ±10% variations in R over the usual range of plasma parameters. The ionization current I_s is obtained by integrating the two-dimensional camera image that corresponds to the core flux tube. The resulting current that is calculated is due to neutral atoms that are ionized; direct molecular processes are not included. Near the plasma edge or at lower electron density and temperature conditions within the core than currently under discussion, R can be as large as 20 to 30 because of molecular processes [2].

C. Particle Balance Measurements

Particle balance measurements during several months of TMX-U operation with various plasma conditions found that above 1 to 3 x

10^{12} cm^{-3}, $I_{\parallel}$ is normally the dominant current channel, and below 1 x 10^{12} cm^{-3} either one or more of the remaining terms ($I_{\perp}^{NA}$, $I_{\perp}^{A}$, q dN/dt) of Eq. (7) dominates the particle balance.

Figure 8 illustrates two cases where the q dN/dt term is small, i.e., no CC buildup. The I_s term obtained from H_α emissions is compared with the total of the directly measured current channels: $I_T \equiv I_{\parallel} + I_{\perp}^{NA} + q\ dN/dt$. The largest contribution to I_T for the Fig. 8a shot is $I_{\parallel}$ (i.e., no axial "plugging" and dN/dt is small after the initial buildup). The disagreement during the initial phase ($t \lesssim 25$ ms) results from changes in radial density profiles during the plasma buildup. In the steady-state

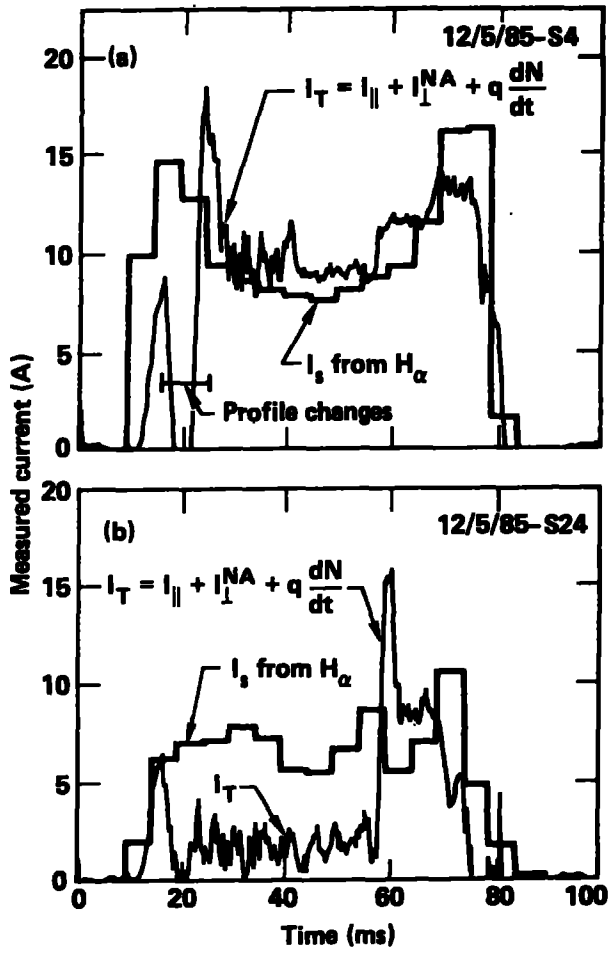

Figure 8. Two examples of negligible q dN/dt. (a) A case where ambipolar transport $I_{\perp}^{A}$ is small. The term I_s derived from the H_α system is nearly equal to I_T; $I_{\parallel}$ is the largest term of I_T. (b) A case where significant $I_{\perp}^{A}$ is present; I_T is greater than I_s until about 60 ms.

phase, the good agreement between I_T and I_s indicates that $I_\perp^A$ is small for these data. This small $I_\perp^A$ also provides a calibration of the experimental method and estimate of the associated errors (~20 to 25%). Under some plasma conditions, however, we observed a significant ambipolar current (see Fig. 8b). For the first 60 ms of this shot, I_s is greater than the total I_T, implying a significant $I_\perp^A$. Just before 60 ms, the CC line density abruptly increases. At nearly this same time, the particle loss current $I_\parallel$ increases so that I_T increases and agrees more closely with I_s. The microwave interferometer signals were noisy during the period where I_s and I_T disagree, suggesting that a low-frequency (~10 kHz) fluctuation was present [8]. This behavior was effectively minimized by controlling machine parameters such as the ICRH power and gas fueling. Although the exact cause of this behavior is uncertain these data illustrate the importance of particle-balance measurements in a tandem mirror, particularly the measurement of the ionization source to obtain $I_\perp^A$.

Figure 9 illustrates a case where q dN/dt is the largest term in I_T. Both $I_\parallel$ and $I_\perp^{NA}$ terms are small with the particle buildup term equal to the particle source (I_s). The plasma heating systems were in the normal

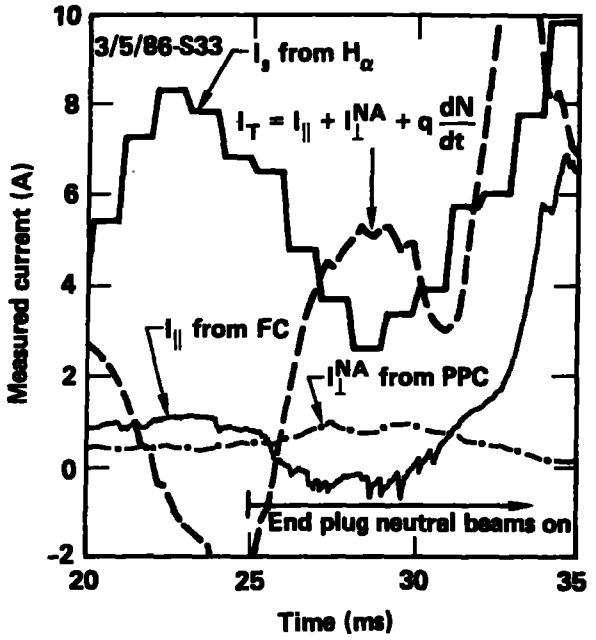

Figure 9. Graph showing each term in the particle balance equation where both $I_\parallel$ and $I_\perp^{NA}$ are small and q dN/dt is positive (26 to 30 ms). Note that $I_T \equiv I_\parallel + I_\perp^{NA} + q\ dN/dt \gtrsim I_s$ starting at 26 ms (when the end-plug beams are turned on), implying small $I_\perp^A$.

thermal-barrier configuration as discussed in the previous section. The ECRH systems were operating at approximately 100 kW (second harmonic at 5 kG) and 60 kW (fundamental at 10 kG); ICRH heating was employed in the central cell. When the sloshing-ion neutral beams within the end cell were turned on 25 ms into the plasma shot, the axial particle loss current $I_{\parallel}$ decreased, as shown in Fig. 9. (The time scale has been expanded to focus on the period where $I_{\parallel}$ and $I_{\perp}^{NA}$ are small.) Note the $I_{\perp}^{NA}$ term is also small because the PPC plates are electrically isolated (10 kΩ relative to ground--a similar shot with grounded PPC plates would yield several amperes of $I_{\perp}^{NA}$). The ionization source I_s and the total I_T are also compared in Fig. 9. During the period of hot-electron buildup (0 to 26 ms), the calculated dN/dt term is first positive (0 to 22 ms), followed by a short period where it is negative (22 to 26 ms); this change may be caused by the constant V assumed in the analysis. After this initial period, the positive dN/dt term offsets the difference between the measured ionization source and the measured particle losses so that $I_T \geq I_s$. We use a constant value of R = 12.0 for these data, which corresponds to the plasma parameters after 28 ms. From 26 to 28 ms, R may be greater because of molecular penetration into the core, but this actually brings I_s closer to I_T. Therefore, within the measurement uncertainties, the outward term $I_{\perp}^{A}$ is small for these data. In addition, both radial and axial loss channels are low during this time (albeit for short duration), and the increase in the measured plasma density is consistent with the increased confinement.

Before leaving this topic of radial transport and total confinement, it should be pointed out that in TMX-U, inward ambipolar transport into the core ($r_c \leq 10$ cm) is not believed to be a problem nor is it required for particle balance because the measured total loss currents are less than or equal to the measured ionization current. Although assumptions about azimuthal symmetry must be made, the same is true at radii beyond the core. However, applying the particle balance equation to the whole CC plasma ($r_c = 25$ cm) shows that I_s is usually greater than I_T even before accounting for ionization of molecules; therefore, the particle balance of the entire CC plasma would imply significant values of $I_{\perp}^{A}$ at large CC radii.

IV. CONCLUDING REMARKS

This paper summarizes TMX-U thermal-barrier plasma potential and confinement results (Secs. II and III). Space limitations have not permitted this paper to cover all the results from TMX-U reported in Ref. [1].

The experimental results from TMX-U verified the thermal-barrier concept in terms of the axial potential profiles and the resulting electrostatic enhancement of axial confinement. TMX-U data showed the axial confinement time to scale according to the predicted (Eq. 5) Pastukhov time (Fig. 6) and demonstrated particle balance inside the central-cell radial core along with density buildup until enhanced axial confinement is lost (i.e., loss of plugging) (Fig. 9).

The performance of TMX-U has been summarized in TABLE I through comparison of the maximum operating range between TMX-U and TMX. Many parameters were increased in TMX-U relative to TMX; however, electrostatically enhanced axial confinement (i.e., plugging), which was measured and validated up to central-cell densities in the low 10^{12} cm^{-3} range, could not be accomplished near the 10^{13} cm^{-3} design range.

As to the primary cause(s) of loss of plugging, a consistent description at all densities is not available. The topic of changes in axial potential and associated confinement continued to be one of the primary investigative areas of TMX-U up to the last month of operation. The thermal-barrier, tandem mirror geometry encompasses both Maxwellian velocity distributions of potentially confined ions and electrons and non-Maxwellian velocity distributions of magnetically confined ions and electrons. Presently, we cannot fully explain loss of plugging in terms of the velocity distributions of the above four plasma species and of the phase space loss-boundaries defined by mirror and electrostatic potential confinement. Continued testing of theoretical models which properly connect plasma densities, temperatures, and potentials would require a larger data base where the particle balance (see Sec. III) for all loss channels is known and where the potential profiles (see Sec. II) are measured by diagnostics with a time response and signal sensitivity to follow the temporal changes during loss of plugging.

In closing, TMX-U developed the heating methods and potential diagnostics that allowed the demonstration of the thermal-barrier configuration at modest densities ($\approx 10^{12}$ cm^{-3}). At central-cell densities

greater than 1 to 3 x 10^{12} cm^{-3}, the existing heating systems (neutral beams, ECRH, and ICRH) could not maintain the potential profile necessary to provide electrostatic enhancement (plugging) of axial confinement.

ACKNOWLEDGMENTS

Most of the material covered in this paper comes from the TMX-U Final Report [1] with the material in Sec. III from Ref. [2]. The author wishes to acknowledge the input from the authors of the TMX-U Final Report with special thanks to the science editor, Gary Porter and to the following authors of sections, which were invaluable in the preparation of this paper: S. L. Allen, M. R. Carter, and J. H. Foote. A careful reading of the final draft with appropriate comments by Dave Hill was extremely helpful. The complete author list of the TMX-U Final Report is: S. L. Allen, D. E. Baldwin, J. D. Barter, L. V. Berzins, M. D. Brown, M. R. Carter, T. A. Casper, J. F. Clauser, F. H. Coensgen, R. H. Cohen, D. L. Correll, W. F. Cummins, C. C. Damm, G. Dimonte, B. H. Failor, S. Falabella, J. H. Foote, A. Friedman, A. H. Futch, R. K. Goodman, D. P. Grubb, L. S. Hall, D. N. Hill, E. B. Hooper, R. S. Hornady, R. D. Horton, W. L. Hsu, B. Huff, A. L. Hunt, R. A. James, R. A. Jong, T. B. Kaiser, C. J. Lasnier, C. A. Leavitt, Y. Matsuda, W. H. Meyer, J. M. Moller, A. W. Molvik, W. E. Nexsen, W. M. Nevins, D. E. Perkins, W. L. Pickles, P. A. Pincosy, P. Poulsen, M. E. Rensink, D. B. Ress, B. W. Rice, M. Shiho, E. H. Silver, T. C. Simonen, B. W. Stallard, J. J. Stewart. W. C. Turner, R. D. Wood, and T. L. Yu.

REFERENCES

[1] G. D. Porter, Ed., TMX-U Final Report, Lawrence Livermore National Laboratory, Livermore, CA, UCID-20981 (1987).

[2] S. L. Allen et al., Determination of Ambipolar Radial Transport in the TMX-U Tandem Mirror, Lawrence Livermore National Laboratory, Livermore, CA, UCRL-94588 (1986), accepted for publication in Nucl. Fusion.

[3] D. E. Baldwin and B. G. Logan, "Improved Tandem Mirror Fusion Reactor," Phys. Rev. Lett. 43, 1318 (1979).

[4] D. L. Correll et al., "Ambipolar Potential Formation and Axial Confinement in TMX," Nucl. Fusion 22, 223 (1982).

[5] T. C. Simonen et al., "Operation of the Tandem-Mirror Plasma Experiment with Skew Neutral-Beam Injection," Phys. Rev. Lett. 50, 1668 (1983).

[6] D. P. Grubb et al., "Thermal Barrier Production and Identification in a Tandem Mirror," Phys. Rev. Lett. 53, 783 (1984).

[7] T. C. Simonen, Ed., Summary of TMX-U Results: 1984, Lawrence Livermore National Laboratory, Livermore, CA, UCID-20274 (1984).

[8] T. A. Casper, Microstability of the TMX Tandem Mirror Experiments, Lawrence Livermore National Laboratory, Livermore, CA, UCRL-96668 (1987). Presented at this Course/Workshop, "Physics of Mirrors, Reversed Field Pinches, and Compact Tori," Varenna, Italy (Sept. 1-11, 1987).

[9] TMX Group, Summary of Results from the Tandem Mirror Experiment (TMX), Lawrence Livermore National Laboratory, Livermore, CA, UCRL-53120, (1981).

[10] W. M. Nevins et al., A Tandem Mirror Modeling Code, Lawrence Livermore National Laboratory, Livermore, CA, UCRL-94436 (1986).

[11] For continuity, this paper uses the same notation for ϕ as used in previous workshops. For reasons of exactness, Ref. [1] uses ϕ to represent potentials at one axial location with respect to the end-wall potential and $\delta\phi$ to represent potential differences between two different axial locations.

[12] M. R. Carter, Potential Measurements in TMX-U Using a Time-of-Flight Analyzer, PhD Thesis, Dept. of Applied Science, Lawrence Livermore National Laboratory, Livermore, CA (1987).

[13] J. H. Foote et al., "TMX-U End-Loss-Ion-Spectrometer," Rev. Sci. Instrum. 57, 1786 (1986).

[14] T. D. Rognlien and T. A. Cutler, "Transition from Collisional to Pastukhov Confinement in Tandem Mirrors, " Nucl. Fusion 20, 1003 (1980).

[15] G. Dimonte, "Nonambipolar Radial Transport in TMX-U," to be published in Bull. Amer. Phys. Soc. (1987) 29th Annual Meeting of APS-DPP.

[16] R. P. Drake et al., "Radial Transport in the TMX Central Cell," Phys. Fluids 25, 2110 (1982).

[17] E. B. Hooper et al., "Nonambipolar Radial Transport in TMX-U," Phys. Fluids 28, 3609 (1985).